

RESEARCH ARTICLE | JANUARY 10 2014

Pressurizing the HgCr_2Se_4 spinel at room temperature

Ilias Efthimiopoulos; Alexander Yaresko; Vladimir Tsurkan; Joachim Deisenhofer; Alois Loidl; Changyong Park; Yuejian Wang

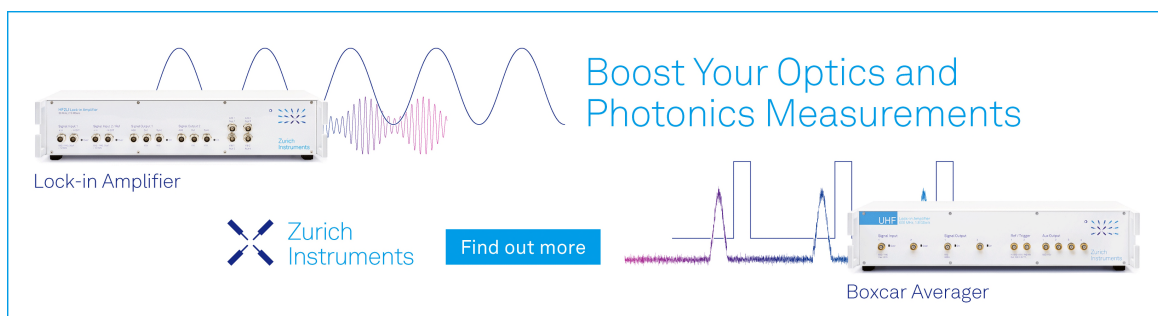
 Check for updates

Appl. Phys. Lett. 104, 011911 (2014)


<https://doi.org/10.1063/1.4861591>



Boost Your Optics and Photonics Measurements



Lock-in Amplifier



Find out more

Boxcar Averager

Pressurizing the HgCr_2Se_4 spinel at room temperature

Ilias Efthimiopoulos,¹ Alexander Yaresko,² Vladimir Tsurkan,^{3,4} Joachim Deisenhofer,³ Alois Loidl,³ Changyong Park,⁵ and Yuejian Wang^{1,a)}

¹Department of Physics, Oakland University, Rochester, Michigan 48309, USA

²Max Planck Institute for Solid State Research, D-70569 Stuttgart, Germany

³Experimental Physics 5, Center for Electronic Correlations and Magnetism, Institute of Physics, University of Augsburg, D-86159 Augsburg, Germany

⁴Institute of Applied Physics, Academy of Sciences of Moldova, MD-2028, Chisinau, Republic of Moldova

⁵High Pressure Collaborative Access Team, Geophysical Laboratory, Carnegie Institution of Washington, Argonne, Illinois 60439, USA

(Received 30 November 2013; accepted 20 December 2013; published online 10 January 2014)

The cubic HgCr_2Se_4 spinel undergoes two structural transitions upon pressure increase. Initially, the ambient-pressure $Fd-3m$ phase transforms into a tetragonal $I4_1/amd$ structure above 15 GPa. We speculate that this $Fd-3m-I4_1/amd$ transition is accompanied by an insulator-to-metal transition, resulting in the vanishing of the Raman signal after the structural transformation. Further compression of HgCr_2Se_4 leads to structural disorder beyond 21 GPa. Our spin-resolved band structure calculations reveal significant changes in the electronic structure of HgCr_2Se_4 after the $Fd-3m-I4_1/amd$ transition, whereas the ferromagnetic interactions are found to dominate in both structures. © 2014 AIP Publishing LLC. [<http://dx.doi.org/10.1063/1.4861591>]

Transition metal compounds (TMCs) constitute one of the most important and fascinating class of solids, exhibiting a wide variety of structures and physical properties.^{1,2} This rich diversity of the physical properties of TMCs results from the unique nature of the outer d -electrons of the transition metal ions with different oxidation states.³ Highlighted examples of the intriguing phenomena displayed by TMCs include the high-temperature superconductivity of cuprates and Fe-based compounds,^{2,4} as well as the colossal magnetoresistance of Mn-bearing perovskites.^{2,5}

Among the plethora of TMCs, Cr-based $\text{ACr}^{3+}_2\text{X}_4$ spinels ($\text{A}^{2+} = \text{Mg, Zn, Cd, Hg}$; $\text{X}^{2-} = \text{O, S, Se}$) with non-magnetic A cations establish a prototype system for studying magnetic exchange interactions in solids.^{6–8} Due to the presence of the magnetic Cr^{3+} cations in a pyrochlore lattice, strong geometric frustration is active in these systems. The strong interplay between magnetism and structure is well documented for these Cr-spinels via the significant spin-phonon coupling^{7,9–13} and the coupled magneto-structural transitions at low temperatures.^{14–17} Furthermore, and adding to this physical complexity, changes of the optical band gap^{18–20} and multiferroicity^{21–24} have been reported for these compounds upon entering magnetically ordered states. This strong interrelation between the lattice, electronic, magnetic, and polar degrees of freedom calls for additional investigations in this series of materials.

Pressure is an effective and “clean” means of tuning the physical properties of Cr-based spinels, with several interesting effects arising upon compression. In particular, pressure can affect the magnitude of ferromagnetic (FM) and antiferromagnetic (AFM) exchange interactions in these compounds, by enhancing the AFM over the FM ones.^{25–28} Another interesting pressure-induced effect is the realization of novel structures,^{29–38} often exhibiting higher cationic

coordinations and completely different physical properties with respect to the starting spinel materials.

In this study, we focus on the ferromagnetic and insulating HgCr_2Se_4 spinel. Earlier high-pressure resistivity measurements revealed an insulator-to-metal transition occurring at ~ 1.7 GPa;³⁹ a recent theoretical study places this pressure-induced band gap closure around 10 GPa.⁴⁰ Partly motivated by this electronic effect, we have conducted high-pressure x-ray diffraction and Raman spectroscopic studies on HgCr_2Se_4 , in order to resolve the role of the structure in the vicinity of the reported insulator-to-metal transition. We have clearly identified two structural transitions: the starting cubic $Fd-3m$ phase adopts a tetragonal $I4_1/amd$ structure at 15 GPa (first-order transition), whereas pressure-induced disorder is observed beyond 21 GPa. We support the experimental results with spin-resolved band structure calculations for both the $Fd-3m$ and the $I4_1/amd$ phases, thus gaining insight on the effect of pressure on the electronic and magnetic properties of HgCr_2Se_4 .

The HgCr_2Se_4 single crystals have been grown by chemical transport reactions using a preliminary synthesized polycrystals as starting materials. The growth process was done between the temperatures 735 and 695 °C, using anhydrous AlCl_3 as the transport agent. The polycrystalline powder was synthesized from the high-purity elements Cr (99.99%) and Se (99.999%) and binary HgSe (99.99%) at a temperature of 700 °C. To reach full reaction, three repeated synthesis cycles were performed. X-ray powder diffraction (XRPD) analysis has not detected the presence of any non-reacted starting materials. Pressure was generated with a gasketed diamond anvil cell, equipped with a set of diamonds with 300 μm culet diameter. The ruby luminescence method⁴¹ was employed for measuring pressure. The high-pressure XRPD measurements were performed at the 16BM-D beamline of the High Pressure Collaborative Access Team, at the Advanced Photon Source of Argonne National Laboratory.

^{a)}Corresponding author. Email ywang235@oakland.edu

Helium served as a pressure transmitting medium (PTM). The XRPD diffractograms were processed with the FIT2D software.⁴² Refinements were performed using the GSAS + EXPGUI software packages.^{43,44} The high-pressure Raman experiments were conducted on single-crystalline HgCr_2Se_4 samples, with helium and a mixture of methanol-ethanol-water 16:3:1, serving as PTM in separate runs. The local spin density approximation (LSDA)-based band structure and magnetic exchange calculations were performed for the experimentally determined crystal structures, using the Linear Muffin-tin Orbitals (LMTO) method,⁴⁵ as implemented in the PY LMTO computer code.⁴⁶ A thorough description of the theoretical methods utilized in this work can be found in Refs. 8 and 47

In Fig. 1(a), we present XRPD patterns of HgCr_2Se_4 at selected pressures. Two structural transitions can be observed upon compression: the starting $Fd-3m$ structure transforms into a tetragonal $I4_1/amd$ phase at 15 GPa. Upon further pressure increase, the XRPD patterns of HgCr_2Se_4 are dominated by a broad peak located at $\sim 10^\circ$ above 21 GPa [Fig. 1(a)], indicative of pressure-induced structural disorder and/or amorphization. Rietveld refinements were performed for both the $Fd-3m$ and $I4_1/amd$ phases, i.e., both the lattice and the interatomic parameter evolution against pressure could be acquired.⁴⁸

The first high-pressure phase is evidenced by the appearance of novel Bragg peaks in the XRPD patterns above 15 GPa; this novel structure has been indexed with the tetragonal $I4_1/amd$ space group ($Z=4$), a direct subgroup of the starting SG $Fd-3m$. The $I4_1/amd$ structure, which retains the same cationic coordination (fourfold for Hg, sixfold for Cr) as the starting cubic phase, is very common among spinels^{14,49,50} and can be easily derived from SG $Fd-3m$:⁴⁸ the c -axis in the two structures is common, whereas the a_{tet} -axis equals the cubic lattice parameter a_{cub} divided by $2^{1/2}$. In our case, the tetragonal c -axis is compressed by 16% and the a -axis is elongated by 7% with respect to their counterparts in the cubic $Fd-3m$ structure.⁴⁸ This results in a 4% volume change at the cubic-tetragonal transition [Fig. 1(b)],

thus classifying the $Fd-3m-I4_1/amd$ as a first-order transition. Such an observation is quite intriguing for spinels, since the $Fd-3m-I4_1/amd$ transition is expected to exhibit second-order character from space group symmetry considerations alone.⁵⁰

Another interesting feature evidenced at the $Fd-3m-I4_1/amd$ transition is the change in the shape of the CrSe_6 octahedra: the octahedra become compressed along c -axis, whereas they expand on the tetragonal ab -plane. This is evidenced in Fig. 1(c) by the behavior of the two distinct Cr-Se bonds in the $I4_1/amd$ phase. In particular, the Cr-Se(1) bonds, which refer to the apical Se(1) ions along c -axis, adopt a $\sim 6\%$ smaller value than the equatorial Cr-Se(2) bond distance at the transition point. This shape change of the CrSe_6 octahedra heavily implies the presence of underlying electronic effects at the $Fd-3m-I4_1/amd$ structural transition. Interestingly, similar first-order $Fd-3m-I4_1/amd$ structural transitions were observed recently for the FeCr_2O_4 ,³¹ MgCr_2O_4 ,³⁵ and HgCr_2S_4 ⁴⁹ spinels under pressure. In the case of FeCr_2O_4 , the first-order character of the transition was attributed to a pressure-induced Jahn-Teller effect of the Fe^{2+} cations residing in the FeO_4 tetrahedra of the spinel structure.³¹ In the case of the MgCr_2O_4 , HgCr_2S_4 , and HgCr_2Se_4 compounds with orbitally inactive Mg^{2+} and Hg^{2+} cations, however, this explanation seems unlikely. We come back to this point below.

Increasing pressure further results in the gradual disappearance of the $I4_1/amd$ Bragg peaks above 21 GPa. The XRPD patterns are now dominated by a significantly broad feature at about 10° , alongside some low-intensity peaks in the $3^\circ-7^\circ$ 2θ angle range [Fig. 1(a)]. This behavior can most likely be attributed to a pressure-induced structural disorder and/or partial amorphization of HgCr_2Se_4 above 21 GPa. A similar pressure-induced disorder was reported for isostructural ZnCr_2S_4 at ~ 10 GPa.³⁴ Upon decompression, the original $Fd-3m$ structure is recovered [Fig. 1(a)].

In order to probe the lattice dynamics of HgCr_2Se_4 under pressure, especially in the vicinity of the $Fd-3m-I4_1/amd$ transition, we have conducted high-pressure

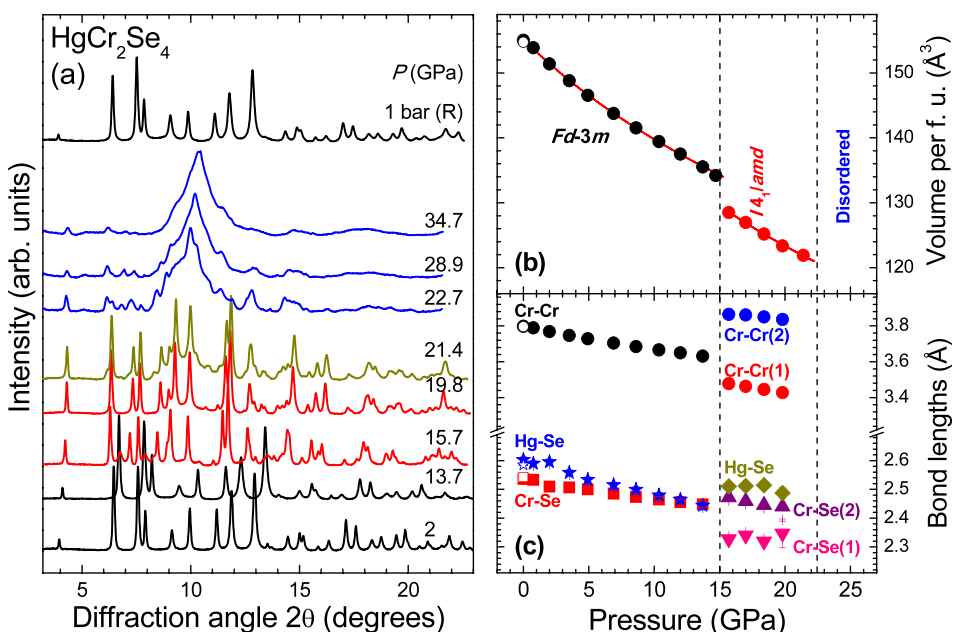


FIG. 1. (a) XRPD patterns of HgCr_2Se_4 at selected pressures ($T = 300$ K, $\lambda = 0.4246$ \AA). The various phases are indicated by different colors: black for $Fd-3m$, red for $I4_1/amd$, blue for the disordered, and dark yellow for the coexistence regime. The pressure dependence of the (b) unit cell volume per formula unit as a function of pressure and (c) selected bond lengths (Cr-Cr, Cr-Se, and Hg-Se) for the cubic $Fd-3m$ and the tetragonal $I4_1/amd$ phases of HgCr_2Se_4 are also displayed. The vertical dashed lines mark the structural transitions.

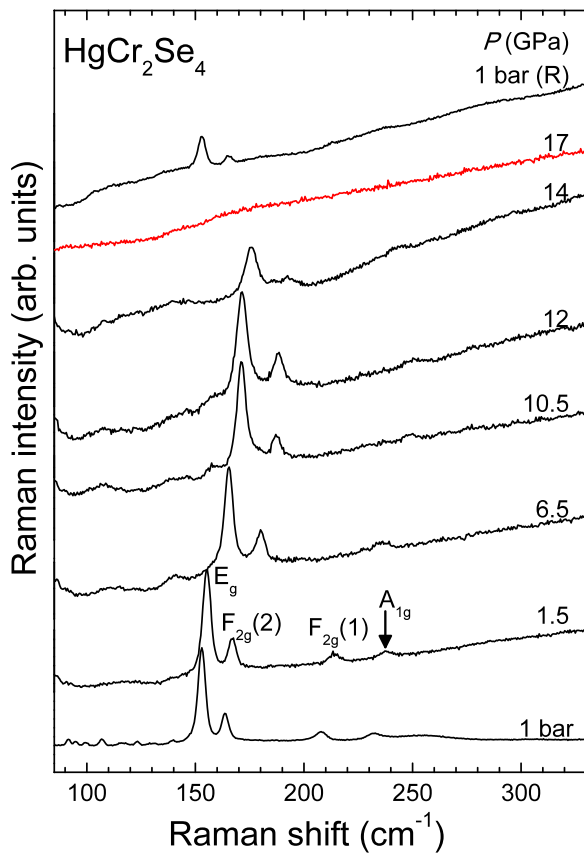


FIG. 2. Selected Raman spectra of HgCr_2Se_4 at various pressures ($\lambda = 532 \text{ nm}$, $T = 300 \text{ K}$). The various phases are indicated by different colors: black for the $Fd-3m$ phase and red for the high-pressure $I4_1/amd$ modification. The Raman mode assignment is displayed.

Raman spectroscopic investigations. The obtained Raman spectra are displayed in Fig. 2. We can observe four Raman-active bands for the $Fd-3m$ phase, with their zero-pressure frequencies ω_0 ⁴⁸ being in good agreement with the reported values.^{51,52} All of the observed Raman modes exhibit “normal” behavior under pressure, with their frequencies increasing monotonously against pressure.⁴⁸

Above 14 GPa, the Raman bands of HgCr_2Se_4 disappear completely, with the Raman spectra becoming rather featureless [Fig. 2]. By taking into account our XRPD study, we attribute this pressure-induced change to the $Fd-3m$ - $I4_1/amd$ structural transition. The starting $Fd-3m$ phase is recovered in the Raman spectra upon decompression (Fig. 2), consistent with the XRPD study [Fig. 1(a)].

For the high-pressure $I4_1/amd$ phase, ten Raman-active modes are expected.⁵³ Even though some degree of local disorder (not evidenced in XRPD) present in the $I4_1/amd$ structure cannot be ruled out as the origin behind the vanishing of the Raman response of HgCr_2Se_4 , we speculate that an electronic effect accompanying the $Fd-3m$ - $I4_1/amd$ structural transition is responsible for the featureless Raman spectra. In particular, a pressure-induced insulator-to-metal transition is known to take place for HgCr_2Se_4 at $\sim 2 \text{ GPa}$.³⁹ Given also that a reduced Raman cross section is expected for metallic systems compared to insulators,⁵⁴ the disappearance of the Raman activity upon passing into the tetragonal phase can most likely be ascribed to a *metallic* $I4_1/amd$ structure. We should point out, however, that the reported

insulator-to-metal transition occurs almost 10 GPa lower than the $Fd-3m$ - $I4_1/amd$ structural transition observed in this work. This significant difference in the transition pressures between the high-pressure transport study of Ref. 39 and our XRPD and Raman experiments can be mainly accounted for by two reasons: (a) the non-hydrostatic nature of the transport measurements under pressure results in the appearance of deviatoric stresses on the sample under investigation, thus yielding generally much lower transition pressures compared to other high-pressure methods,⁵⁵ and (b) the quality of the HgCr_2Se_4 sample employed in each investigation, since it is well documented that the growth conditions of chalcogenide spinels can affect the physical properties significantly.⁵⁶ Interestingly, recent theoretical calculations place the band gap closure of HgCr_2Se_4 at about 10 GPa,⁴⁰ very close to the $Fd-3m$ - $I4_1/amd$ structural transition seen here. Nevertheless, an up-to-date high-pressure resistivity study on HgCr_2Se_4 will be needed to verify a possible insulator-to-metal transition at the $Fd-3m$ - $I4_1/amd$ structural modification.

In order to acquire a qualitative picture of the effect of pressure on the electronic and magnetic properties of HgCr_2Se_4 , we have performed LSDA-based band structure calculations for both the $Fd-3m$ and the high-pressure $I4_1/amd$ phases. Figure 3(a) shows the calculated non-spin polarized Cr-*d* and Se-*p* density of states (DOS) for the $Fd-3m$ structure at three different pressures, i.e., at 0 (blue), 4.9 (green), and 13.7 GPa (red). The width of the Cr *d* and Se *p* states, as well as the ligand-field splitting between the Cr t_{2g} and e_g states increase upon increasing pressure due to the increasing hopping matrix elements. A strong narrow peak of the Cr t_{2g} states is located exactly at E_F , which indicates that HgCr_2Se_4 is close to a structural and/or a magnetic instability. Indeed, in the LSDA calculations for the $Fd-3m$ structure (not shown), the t_{2g} states become completely spin-polarized yielding a Cr magnetic moment of $3 \mu_B$. The non-spin polarized DOS curves calculated for the high-pressure $I4_1/amd$ phase are directly compared to those of the $Fd-3m$ structure ($P = 13.7 \text{ GPa}$) in Fig. 3(b). We can clearly observe that the intense DOS peak at E_F is strongly suppressed upon passing into the $I4_1/amd$ structure, denoting a tendency to suppress magnetism in the high-pressure tetragonal modification of HgCr_2Se_4 . In addition, the inset in Fig. 3(b) shows the orbital configuration of the Cr t_{2g} states for the $I4_1/amd$ phase. The tetragonal distortion of the CrSe_6 octahedra, i.e., “squeezed” along *c*-axis and expanded on the *ab*-plane [Fig. 1(c)], splits the Cr t_{2g} states into almost completely filled dx^2-y^2 and partially occupied *dxy* and *dyz* states (the Cr *d* orbitals are defined in the tetragonal frame).

Turning now to the magnetic properties of HgCr_2Se_4 under pressure, spin-polarized LSDA calculations for the $Fd-3m$ structure give a spin-spiral ground state with a pressure-dependent incommensurate wave vector \mathbf{q}_{min} .⁴⁸ Some trends in the pressure-induced changes of the magnetic properties of HgCr_2Se_4 can be captured, however, already by comparing the pressure dependence of stabilization energies ΔE for a commensurate FM and an all-in all-out zero-moment (ZM) order (Fig. 4). In the latter, the Cr magnetic moments point either towards or away from the center of a Cr_4 tetrahedron in equal proportion, which results in a zero net magnetic moment.⁴⁸ Figure 4 shows that the energy

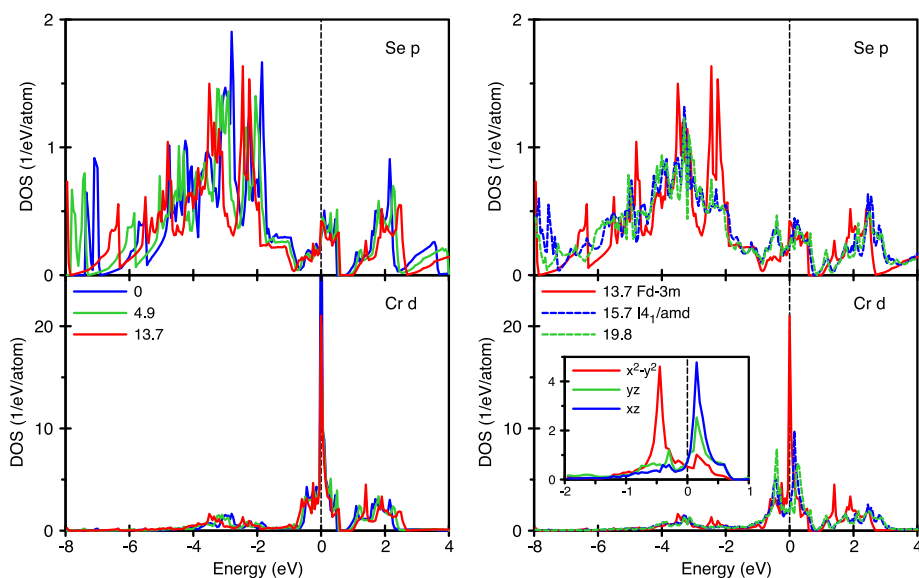


FIG. 3. (Left) Non-spin polarized Cr *d* and Se *p* DOS for the *Fd-3m* structure. Zero energy is at the Fermi level (E_F). The DOS peaks at E_F and at ~ 2 eV originate from Cr t_{2g} and e_g states, respectively. (Right) Direct comparison between the Cr *d* and Se *p* DOS for the *Fd-3m* ($P = 13.7$ GPa) and $I4_1/amd$ ($P = 15.7$ and 19.8 GPa) structures. Inset shows densities of the Cr t_{2g} states split by tetragonal distortions.

gain caused by the formation of a magnetic state is gradually suppressed by increasing pressure. Magnetic solutions were also obtained for the tetragonal $I4_1/amd$ structure, for which collinear antiferromagnetic order was considered instead of the ZM one.⁴⁸ However, the stabilization energies are strongly reduced after the *Fd-3m*- $I4_1/amd$ structural transition. The energy difference between the FM and the ZM/AFM solutions decreases with pressure, which indicates weakening of a FM contribution to the nearest neighbor exchange interaction j_1 . Nevertheless, the FM solution remains always more favorable energetically than the ZM/AFM one at all pressures.

It should be mentioned that the LSDA spin-spiral calculations for the cubic $HgCr_2Se_4$ yield a metallic solution at small \mathbf{q} (including \mathbf{q}_{min}) for all pressures. The insulating behavior at ambient pressure⁵⁷ can be reproduced though, if one accounts for the relatively strong electronic correlations in the Cr *d* shell by performing LDA + *U* calculations. A *U* value of 2 eV is sufficient in order to open a gap at \mathbf{q}_{min} at ambient pressure. Even though not attempted here, a pressure-induced band crossing between majority and minority spin states has been reported for the *Fd-3m* phase of $HgCr_2Se_4$ above 10 GPa in a recent theoretical work.⁴⁰ This

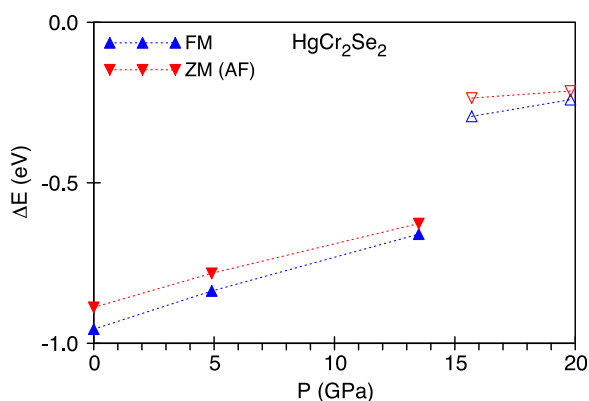


FIG. 4. Pressure dependence of the magnetic energies ΔE for the FM (blue) and ZM (red) structures of $HgCr_2Se_2$. The magnetic energy is defined as $\Delta E = E_M - E_0$, where E_M and E_0 are the total energies obtained for a spin-polarized and a spin-restricted solution, respectively.

band gap closure was rationalized within the context of a pressure-induced insulator-to-metal transition. Therefore, it appears that the *Fd-3m*- $I4_1/amd$ structural transition of $HgCr_2Se_4$ at 15 GPa is accompanied by an insulator-to-metal transition, consistent with the vanishing of the Raman response of the material after adoption of the tetragonal phase (Fig. 2). This pressure-induced band gap closure alone, however, cannot account for the first-order character of the *Fd-3m*- $I4_1/amd$ structural transition [Fig. 1(b)]. More effort will be required in order to understand the underlying microscopic effects in the vicinity of this structural transition.

Finally, we would like to discuss the structural disorder observed for $HgCr_2Se_4$ beyond 21 GPa [Fig. 1(a)]. Generally, pressure-induced disorder can be accounted for by two mechanisms:⁵⁸ (a) the disordered phase may be a transient of a structural transition into another crystalline phase, which cannot form properly due to kinetic barriers or (b) the tendency of the material to decompose into its constituents. Due to the reversibility of the starting *Fd-3m* phase upon decompression [Fig. 1(a)], however, we tend to exclude the decomposition scenario. Therefore, we propose that this disordered structure of $HgCr_2Se_4$ appearing above 21 GPa is a precursor of another crystalline phase, which probably exhibits higher cationic coordinations. Considering the available literature on spinel compounds, we can suggest the following candidates as possible structures for this second high-pressure phase of $HgCr_2Se_4$: (I) a Cr_3S_4 -type structure, which is the high-pressure phase of $FeCr_2S_4$ ²⁹ (sixfold coordination of both cations) and a common polymorph for several sulphide and selenide Cr-spinels at combined high-pressure and high-temperature conditions,^{33,36–38} (II) one of the monoclinic high-pressure phases reported recently for Co_3O_4 ⁵⁹ (sixfold coordination for both cations), or (III) one of the denser $CaFe_2O_4$ -, $CaMn_2O_4$ -, and $CaTi_2O_4$ -type structures (eightfold and sixfold cationic coordinations) adopted by several oxide spinels upon compression with or without thermal treatment.^{30,32} Nevertheless, a combined high-pressure and high-temperature structural study on $HgCr_2Se_4$ will be needed in order to identify this disordered structure.

In conclusion, we have shown that the cubic $HgCr_2Se_4$ spinel undergoes two structural transitions upon pressure increase. In particular, the ambient-pressure *Fd-3m* structure

transforms into a tetragonal $I4_1/amd$ phase above 15 GPa. By taking into account an earlier high-pressure resistivity study,³⁹ a recent theoretical investigation,⁴⁰ and the vanishing of the Raman signal after the $Fd-3m-I4_1/amd$ structural transformation, we speculate that this $Fd-3m-I4_1/amd$ transition of $HgCr_2Se_4$ is accompanied by an insulator-to-metal transition. Our band structure calculations demonstrate the significant Cr-*d* DOS rearrangement after the $Fd-3m-I4_1/amd$ transition. Furthermore, the ferromagnetic nearest neighbor magnetic exchange interaction is shown to prevail in both the $Fd-3m$ and the $I4_1/amd$ phases. Upon further compression, $HgCr_2Se_4$ undergoes pressure-induced disorder beyond 21 GPa. We interpret this behavior as a precursor of another crystalline phase with higher cationic coordinations, which cannot crystallize properly due to kinetic effects. A more detailed characterization of the structural properties of $HgCr_2Se_4$ above 21 GPa involving *in situ* temperature treatment is left for future investigations.

Portions of this work were performed at HPCAT (Sector 16), Advanced Photon Source (APS), and Argonne National Laboratory (ANL). HPCAT operations are supported by DOE-NNSA under Award No. DE-NA0001974 and DOE-BES under Award No. DE-FG02-99ER45775, with partial instrumentation funding by NSF. APS is supported by DOE-BES, under Contract No. DE-AC02-06CH11357. Compressed neon and helium gas loadings were performed at GeoSoilEnviroCARS (Sector 13), APS-ANL. GeoSoilEnviroCARS is supported by the National Science Foundation-Earth Sciences (No. EAR-0622171) and Department of Energy-Geosciences (No. DE-FG02-94ER14466). We would like to acknowledge Dr. S. Tkachev at GSECARS for his help with the DAC gas loading. This research has been partially supported by the DFG via TRR 80 (Augsburg-Munich) and faculty research fellowship from Oakland University.

¹C. N. R. Rao and K. P. R. Pisharody, *Prog. Solid State Chem.* **10**, 207 (1976).
²C. N. R. Rao and B. Raveau, *Transition Metal Oxides*, 2nd ed. (John Wiley & Sons, Inc., 1998).
³H. L. Schlaefler and G. Gliemann, *Basic Principles of Ligand Field Theory* (Wiley Interscience, 1969).
⁴T. Tohyama, "Recent Progress in Physics of High-Temperature Superconductors," *Jpn. J. Appl. Phys. Part 1* **51**, 010004 (2012).
⁵M. B. Salamon and M. Jaime, *Rev. Mod. Phys.* **73**, 583 (2001).
⁶P. K. Baltzer, P. J. Wojtowicz, M. Robbins, and E. Lopatin, *Phys. Rev.* **151**, 367 (1966).
⁷T. Rudolf, C. Kant, F. Mayr, J. Hemberger, V. Tsurkan, and A. Loidl, *New J. Phys.* **9**, 76 (2007).
⁸A. N. Yaresko, *Phys. Rev. B* **77**, 115106 (2008).
⁹T. Rudolf, C. Kant, F. Mayr, J. Hemberger, V. Tsurkan, and A. Loidl, *Phys. Rev. B* **75**, 52410 (2007).
¹⁰T. Rudolf, C. Kant, F. Mayr, J. Hemberger, V. Tsurkan, and A. Loidl, *Phys. Rev. B* **76**, 174307 (2007).
¹¹J. Hemberger, T. Rudolf, H.-A. K. von Nidda, F. Mayr, A. Pimenov, V. Tsurkan, and A. Loidl, *Phys. Rev. Lett.* **97**, 87204 (2006).
¹²V. Gnezdilov, P. Lemmens, Y. G. Pashkevich, C. Payen, K. Y. Choi, J. Hemberger, A. Loidl, and V. Tsurkan, *Phys. Rev. B* **84**, 45106 (2011).
¹³V. Felea, S. Yasin, A. Gunther, J. Deisenhofer, H.-A. K. von Nidda, S. Zherlitsyn, V. Tsurkan, P. Lemmens, J. Wosnitza, and A. Loidl, *Phys. Rev. B* **86**, 104420 (2012).
¹⁴F. Yokaichiya, A. Krimmel, V. Tsurkan, I. Margiolaki, P. Thompson, H. N. Bordallo, A. Buchsteiner, N. Stuesser, D. N. Argyriou, and A. Loidl, *Phys. Rev. B* **79**, 64423 (2009).
¹⁵L. Ortega-San-Martin, A. J. Williams, C. D. Gordon, S. Klemme, and J. P. Attfield, "Low temperature neutron diffraction study of $MgCr_2O_4$ spinel," *J. Phys. Condens. Matter* **20**, 104238 (2008).

¹⁶M. Hidaka, M. Yoshimura, N. Tokiwa, J. Akimitsu, Y. J. Park, J. H. Park, S. D. Ji, and K. B. Lee, "Structural modulation induced by the incommensurate antiferromagnetic phase transition in $ZnCr_2Se_4$," *Phys. Stat. Sol. (b)* **236**, 570 (2003).
¹⁷H. Gobel, *J. Magn. Magn. Mater.* **3**, 143 (1976).
¹⁸H. W. Lehmann and G. Harbeke, *Phys. Rev. B* **1**, 319 (1970).
¹⁹H. W. Lehmann and M. Robbins, *J. Appl. Phys.* **37**, 1389 (1966).
²⁰L. Goldstein, P. Gibart, and A. Selmi, *J. Appl. Phys.* **49**, 1474 (1978).
²¹J. Hemberger, P. Lunkenheimer, R. Fichtl, S. Weber, V. Tsurkan, and A. Loidl, *Phase Transform.* **79**, 1065 (2006).
²²J. Hemberger, P. Lunkenheimer, R. Fichtl, S. Weber, V. Tsurkan, and A. Loidl, *Physica B* **378**, 363 (2006).
²³J. Hemberger, P. Lunkenheimer, R. Fichtl, H.-A. K. von Nidda, V. Tsurkan, and A. Loidl, *Nature* **434**, 364 (2005).
²⁴S. Weber, P. Lunkenheimer, R. Fichtl, J. Hemberger, V. Tsurkan, and A. Loidl, *Phys. Rev. Lett.* **96**, 157202 (2006).
²⁵V. C. Srivastava, *J. Appl. Phys.* **40**, 1017 (1969).
²⁶N. Sakai and J. H. Pifer, *Phys. Rev. B* **33**, 1875 (1986).
²⁷Y. Jo, J.-G. Park, H. C. Kim, W. Ratcliff II, and S.-W. Cheong, *Phys. Rev. B* **72**, 184421 (2005).
²⁸H. Ueda and Y. Ueda, *Phys. Rev. B* **77**, 224411 (2008).
²⁹Y. Amiel, G. K. Rozenberg, N. Nissim, A. Milner, M. P. Pasternak, M. Hanfland, and R. D. Taylor, *Phys. Rev. B* **84**, 224114 (2011).
³⁰A. M. Arevalo-Lopez, A. J. Dos Santos-Garcia, E. Castillo-Martinez, A. Duran, and M. A. Alario-Franco, *Inorg. Chem.* **49**, 2827 (2010).
³¹A. Kyono, S. A. Gramsch, T. Yamanaka, D. Ikuta, M. Ahart, B. O. Mysen, H. K. Mao, and R. J. Hemley, *Phys. Chem. Miner.* **39**, 131 (2012).
³²D. Levy, V. Diella, A. Pavese, M. Dapiaggi, and A. Sani, *Am. Mineral.* **90**, 1157 (2005).
³³M. D. Banus and M. C. Lavine, *J. Solid State Chem.* **1**, 109 (1969).
³⁴J. Wittlinger, S. Werner, and H. Schulz, *Phys. Chem. Miner.* **24**, 597 (1997).
³⁵W. Yong, S. Botis, S. R. Shieh, W. Shi, and A. C. Withers, *Phys. Earth Planet. Inter.* **196-197**, 75 (2012).
³⁶R. J. Bouchard, *Mater. Res. Bull.* **2**, 459 (1967).
³⁷W. Albers and C. J. M. Rooymans, *Solid State Commun.* **3**, 417 (1965).
³⁸P. Vaqueiro, A. V. Powell, S. Hull, and D. A. Keen, *Phys. Rev. B* **63**, 64106 (2001).
³⁹P. Kistaiah, K. S. Murthy, and K. V. K. Rao, *J. Less-Common Met.* **98**, L13 (1984).
⁴⁰S.-D. Guo and B.-G. Liu, "Density-functional-theory investigation of pressure induced semiconductor-metal transitions in the ferromagnetic semiconductor $HgCr_2Se_4$," *J. Phys.: Condens. Matter* **24**, 045502 (2012).
⁴¹H. K. Mao, J. Xu, and P. Bell, *J. Geophys. Res.* **91**, 4673, doi:10.1029/JB091iB05p04673 (1986).
⁴²A. Hammersley, S. Svensson, M. Hanfland, A. Fitch, and D. Hausermann, *High Pressure Res.* **14**, 235 (1996).
⁴³B. H. Toby, *J. Appl. Crystallogr.* **34**, 210 (2001).
⁴⁴R. B. von Dreele and A. C. Larson, Los Alamos National Laboratory Report No. LAUR 86-748, 1994.
⁴⁵O. K. Andersen, *Phys. Rev. B* **12**, 3060 (1975).
⁴⁶A. Y. Perlov, A. N. Yaresko, and V. N. Antonov, "PY-LMTO, A Spin-polarized Relativistic Linear Muffin-tin Orbitals Package for Electronic Structure Calculations" (unpublished).
⁴⁷A. V. Ushakov, D. A. Kukusta, A. N. Yaresko, and D. I. Khomskii, *Phys. Rev. B* **87**, 14418 (2013).
⁴⁸See supplementary material at <http://dx.doi.org/10.1063/1.4861591> for complementary structural and Raman-related data, as well as for additional information on the magnetic structure calculations.
⁴⁹I. Efthimiopoulos, A. Yaresko, V. Tsurkan, J. Deisenhofer, A. Loidl, C. Park, and Y. Wang, *Appl. Phys. Lett.* **103**, 201908 (2013).
⁵⁰P. G. Radaelli, *New J. Phys.* **7**, 53 (2005).
⁵¹A. K. Kushwaha, *Commun. Theor. Phys.* **50**, 1422 (2008).
⁵²M. N. Iliev, E. Anastassakis, and T. Arai, "Raman scattering of $HgCr_2Se_4$," *Phys. Stat. Solidi (b)* **86**, 717 (1978).
⁵³C. M. Julien and M. Massot, "Raman spectroscopic studies of lithium manganese with spinel structure," *J. Phys.: Condens. Matter* **15**, 3151 (2003).
⁵⁴A. F. Goncharov and V. V. Struzhkin, *J. Raman Spectrosc.* **34**, 532 (2003).
⁵⁵M. I. Eremets, *High Pressure Experimental Methods* (Oxford Science Publications, 1996).
⁵⁶K. G. Nikiforov, "Magnetically ordered multinary semiconductors," *Prog. Cryst. Growth Charact. Mater.* **39**, 1 (1999).
⁵⁷H. W. Lehmann and F. P. Emmenegger, *Solid State Commun.* **7**, 965 (1969).
⁵⁸S. M. Sharma and S. K. Sikka, *Prog. Mater. Sci.* **40**, 1 (1996).
⁵⁹S. Hirai and W. L. Mao, *Appl. Phys. Lett.* **102**, 41912 (2013).